Supporting Information for:

(De)localization dynamics of molecular excitons: comparison of mixed quantum-classical and fully quantum treatments

Evgenii Titov[‡], Tristan Kopp, Joscha Hoche, Alexander Humeniuk, and Roland Mitrić*

Institut für Physikalische und Theoretische Chemie, Julius-Maximilians-Universität Würzburg, Emil-Fischer-Straße 42, 97074 Würzburg, Germany

*roland.mitric@uni-wuerzburg.de

Contents

[‡] Present address: Theoretical Chemistry, Institute of Chemistry, University of Potsdam, Karl-Liebknecht-Straße 24-25, 14476 Potsdam, Germany.

SI1 Excited state calculations

The low-lying excited states of the dimer shown in Fig. 1 of the main text have been first investigated using TD-DFT[S1] and wave function based methods. Specifically, three density functional approximations (global hybrid B3LYP,[S2,S3] Coulomb-attenuated range-separated CAM-B3LYP,[S4] and long-range corrected ωB97X-D[S5]), TD-HF,[S6] ADC(2)[S7] and CC2[S8] have been employed. TD-DFT and TD-HF calculations have been performed with Gaussian 16,[S9] ADC(2) and CC2 calculations with TURBOMOLE V7.0.[S10] The vertical excitation energies and corresponding oscillator strengths are shown in Tab. S1.

Table S1: Excitation wavelengths (λ in nm), excitation energies (ΔE in eV), and oscillator strengths (f) for the first six electronic transitions[a]

	TD-B3LYP[b]			TD-CAM-B3LYP[b]			TD-ωB97X-D[b]			TD-HF[b]			ADC(2)[c]			CC2[c]		
Transition	λ	ΔE	f	λ	ΔE	f	λ	ΔE	f	λ	ΔE	f	λ	ΔE	f	λ	ΔE	f
$S_0 \rightarrow S_1$	524	2.37	0.23	462	2.69	0.36	454	2.73	0.39	430	2.88	0.58	431	2.88	0.43	429	2.89	0.36
$S_0 \rightarrow S_2$	515	2.41	0.00	453	2.74	0.00	445	2.79	0.00	418	2.97	0.00	424	2.93	0.00	422	2.94	0.00
$S_0 \rightarrow S_3$	513	2.42	0.00	341	3.64	0.00	338	3.67	0.00	315	3.94	0.00	347	3.57	0.00	347	3.57	0.00
$S_0 \rightarrow S_4$	513	2.42	0.00	341	3.64	0.00	338	3.67	0.00	315	3.94	0.00	347	3.58	0.00	347	3.57	0.00
$S_0 \rightarrow S_5$	363	3.42	0.00	323	3.84	0.00	299	4.15	0.00	276	4.49	0.00	335	3.70	0.00	339	3.66	0.00
$S_0 \rightarrow S_6$	363	3.42	0.00	323	3.84	0.00	297	4.18	0.01	274	4.53	0.01	335	3.70	0.00	339	3.66	0.00
	TD-DFTB			TD-lc-DFTB			TD-lc-DFTB (100×100)[d]			TD-lc-DFTB (90×90)[d]			TD-lc-DFTB (80×80)[d]			TD-lc-DFTB (70×70)[d]		
Transition	λ	ΔE	f	λ	ΔE	f	λ	ΔE	f	λ	ΔE	f	λ	ΔE	f	λ	ΔE	f
$S_0 \rightarrow S_1$	507	2.45	0.00	401	3.09	0.47	395	3.14	0.49	392	3.16	0.50	389	3.19	0.51	385	3.22	0.52
$S_0 \rightarrow S_2$	507	2.45	0.00	391	3.17	0.00	383	3.24	0.00	381	3.26	0.00	377	3.29	0.00	373	3.33	0.00
$S_0 \rightarrow S_3$	427	2.91	0.33	308	4.03	0.00	307	4.04	0.00	307	4.04	0.00	306	4.05	0.00	306	4.05	0.00
$S_0 \rightarrow S_4$	419	2.96	0.00	306	4.05	0.25	306	4.06	0.24	305	4.06	0.24	305	4.06	0.23	305	4.07	0.23
$S_0 \rightarrow S_5$	320	3.87	0.00	283	4.38	0.00	279	4.44	0.00	278	4.46	0.00	277	4.48	0.00	275	4.51	0.00
$S_0 \rightarrow S_6$	320	3.87	0.00	280	4.42	0.00	276	4.48	0.00	275	4.51	0.00	274	4.53	0.00	272	4.56	0.00
	TD-lc-DFTB (60×60)[d]			TD-lc-DFTB (50×50)[d]			TD-lc-DFTB (40×40)[d]			TD-lc-DFTB (30×30)[d]			TD-lc-DFTB (20×20)[d]			TD-lc-DFTB (10×10)[d]		
Transition	λ	ΔE	f	λ	ΔE	f	λ	ΔE	f	λ	ΔE	f	λ	ΔE	f	λ	ΔE	f
$S_0 \rightarrow S_1$	383	3.24	0.53	382	3.25	0.53	380	3.27	0.55	376	3.30	0.57	373	3.32	0.58	359	3.45	0.50
$S_0 \rightarrow S_2$	370	3.35	0.00	369	3.36	0.00	366	3.39	0.00	361	3.43	0.00	358	3.47	0.00	349	3.56	0.00
$S_0 \rightarrow S_3$	306	4.06	0.00	304	4.07	0.00	304	4.08	0.00	300	4.14	0.00	298	4.15	0.00	283	4.38	0.00
$S_0 \rightarrow S_4$	304	4.07	0.22	303	4.09	0.22	303	4.09	0.21	299	4.15	0.21	298	4.17	0.21	282	4.40	0.24
$S_0 \rightarrow S_5$	274	4.52	0.00	273	4.54	0.00	272	4.55	0.00	271	4.57	0.00	269	4.61	0.00	257	4.82	0.00
$S_0 \rightarrow S_6$	271	4.58	0.00	270	4.60	0.00	269	4.61	0.00	268	4.63	0.00	266	4.67	0.00	254	4.88	0.00

[a] Geometry was optimized at the ωB97X-D/6-31G* level of theory.
[b] With the def2-TZVP basis set.[S11]
[c] With the cc-pVDZ basis set.[S12]
[d] The size of active space (number of highest occupied orbitals × number of lowest virtual orbitals).

The $S_0 \rightarrow S_1$ transition possesses a sizable oscillator strength, whereas the other transitions have oscillator strengths close to zero. The excitation energy of the $S_0 \rightarrow S_1$ transition increases in the order TD-B3LYP (2.37 eV) < TD-CAM-B3LYP (2.69 eV) < TD-ωB97X-D (2.73 eV) < TD-HF (2.88 eV). The blue shift of excitation energies is

expected when adding more exact exchange or introducing long-range correction into a density functional approximation, and this is what we observe for the tetracene dimer under study. The experimental absorption maximum for the toluene solution of the tetracene dimer is located at ∼2.5 eV.[S13] Comparing to this value, we obtain a blue shift of ∼0.2 eV with the range-separated functionals (CAM-B3LYP and ωB97X-D) and a red shift of ∼0.1 eV with B3LYP. We note that the experimental maximum corresponds to the peak in vibrationally resolved absorption spectrum, whereas the computed excitation energies correspond to a vertical excitation. The vertical excitation energy is normally expected to be larger than the corresponding 0-0 energy. Moreover, the solvent effects may also lead to a spectral shift, often a red shift. Therefore we conclude that the range-separated functionals perform better for the excitation energies of the tetracene dimer than B3LYP. In addition, we calculated the absorption spectrum with the ADC(2) and CC2 methods using the cc-pVDZ basis set. The S_1 excitation energy obtained with these methods is (almost) the same as the one calculated with TD-HF/def2-TZVP. This accords with the corresponding results for the trimer, for which this energy is equal to 2.90 eV.[S14]. We note, however, that the exciton splitting between the S_1 and S_2 states is larger for TD-HF (∼0.1 eV) than for ADC(2) and CC2 as well as the range-separated functionals (∼0.05 eV).

The other, even more important issue is to correctly describe the nature of excited states. It is well known that the density functional approximations with a rather small fraction of exact exchange, *e.g.*, B3LYP (20% of exact exchange), suffer from the so-called charge transfer problem.[S15–S18] Namely, such functionals usually produce spurious low-lying charge transfer states or admix charge transfer into local excitations in molecular aggregates, starting from a dimer.[S19–S21] This problem comes out for our B3LYP calculation shown in Tab. S1. In Tab. S1 we immediately note the low oscillator strength of the $S_0 \rightarrow S_1$ transition obtained with TD-B3LYP, as being compared to the results of other methods. Further, inspection of transition density matrix and natural transition orbitals for the $S_0 \rightarrow S_1$ transition clearly indicates the admixture of charge transfer into Frenkel exciton. Thus, to properly describe the nature of low-lying excitonic states one should employ the range-separation strategy or add a larger amount of exact exchange to a global hybrid functional.

We have then investigated how well the TD-lc-DFTB approach performs for the tetracene dimer under consideration. The results of TD-lc-DFTB calculations are shown in Tab. S1 and in Fig. S1. The TD-lc-DFTB $S_0 \rightarrow S_1$ excitation energy is found to be higher than 3 eV, and this energy increases with shrinking active orbital space. At this point one may wonder why the TD-lc-DFTB energies are considerably blue-shifted with respect to those for the tetracene trimer, reported in our earlier work.[S14] Specifically, the TD-lc-DFTB $S_0 \rightarrow S_1$ excitation energy of the tetracene trimer was calculated to be 2.5 eV when using the full active space (180×180) and 2.76 eV with the 30×30 active space (used for the surface hopping dynamics).[S14] The reason for this is a change of the confinement radius for carbon: ∼4.309 a_0 is used here, whereas ∼2.657 a_0 was used in ref. S14. We note that the experimental spectra of the dimer and the trimer are found to be very similar.[S13]

When considering the full active space, the absorption spectrum of the dimer is blue-shifted with respect to the spectrum calculated with the ωB97X-D functional by

∼0.4 eV (see Tab. S1). However, the nature of the lowest excited states is correctly captured with the TD-lc-DFTB method (see Fig. S2). For the dynamics, we use the reduced active space composed of the highest 30 occupied and the lowest 30 virtual orbitals (30×30), that allows one to speed up calculations and at the same time does not lead to considerable deterioration of the excitation energies and oscillator strengths. We also note that TD-DFTB without lc fails to yield correct excitonic states, suffering from the CT problem. From Fig. S1 and Tab. S1 we also see that, when suitable methods are employed, the S_3 state is well separated, by more than 0.5 eV, from the excitonic S_1 and S_2 states.

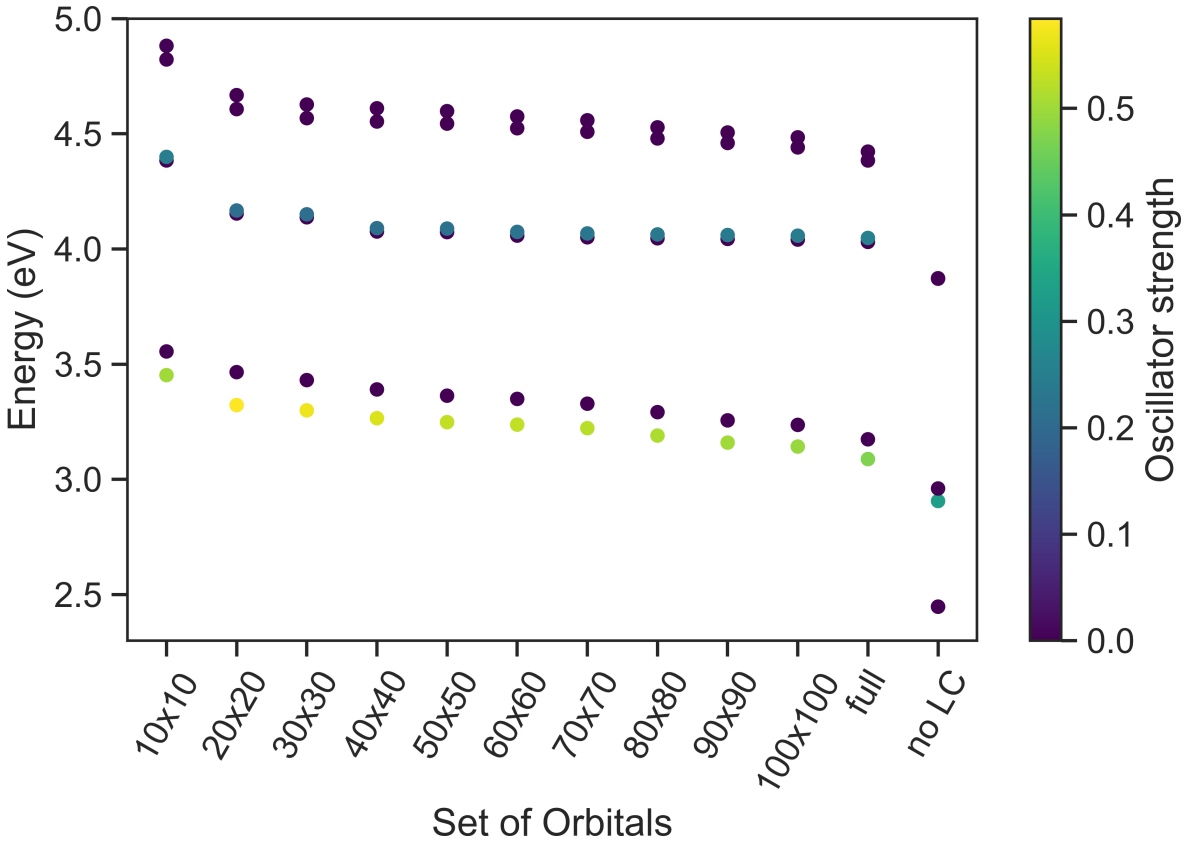

Figure S1: Excitation energies and oscillator strengths for the first six transition computed with TD-lc-DFTB as a function of active space (indicated as `number of occupied orbitals` × `number of virtual orbitals`). The results of the TD-DFTB calculation without lc correction are also shown. "full" means that all occupied (125 in total) and all virtual (125 in total) orbitals were used.

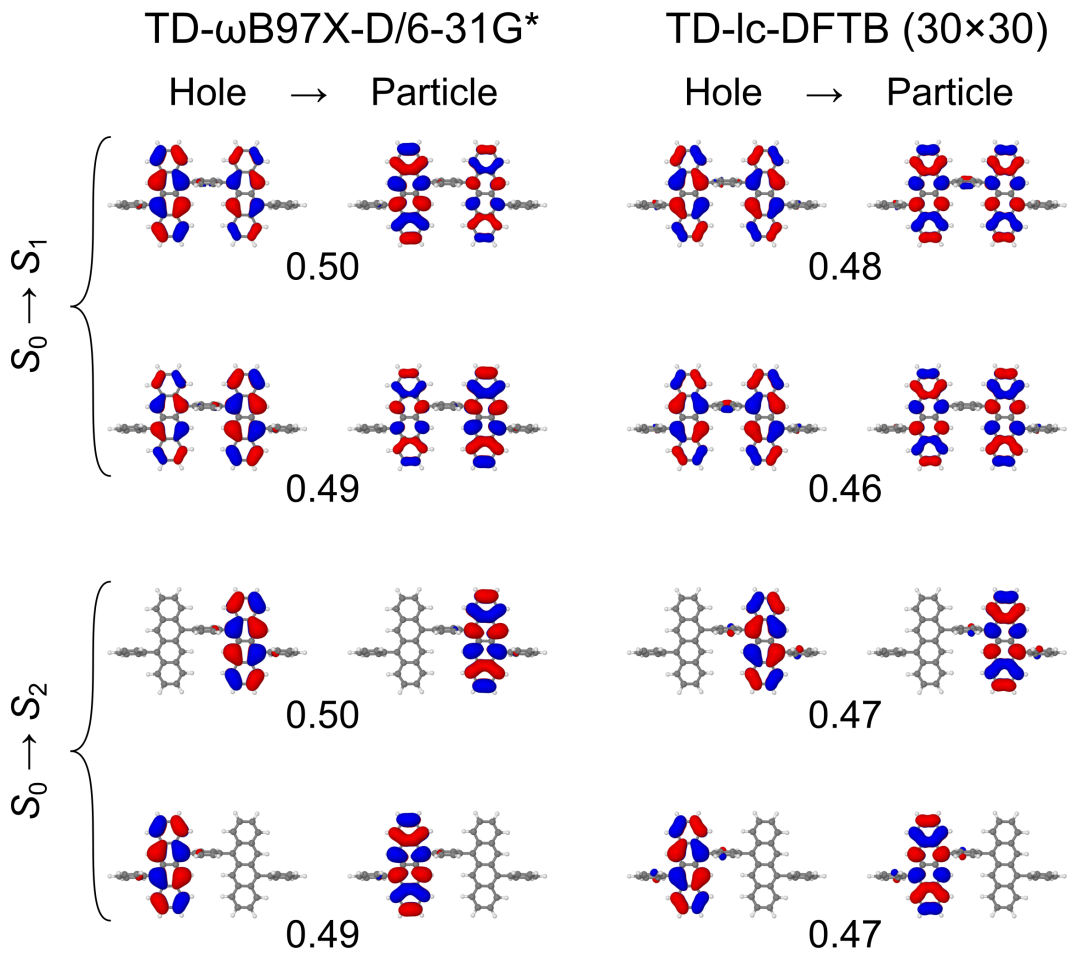

Figure S2: Dominant natural transition orbital (NTO) pairs for the $S_0 \rightarrow S_1$ and $S_0 \rightarrow S_2$ transitions, calculated on the TD-ωB97X-D/6-31G* and TD-lc-DFTB (30×30) levels of theory, at the ωB97X-D/6-31G* ground-state optimized geometry. Numbers are the contributions of NTO hole–electron pairs to a given transition.

SI2 Thermally broadened absorption spectrum

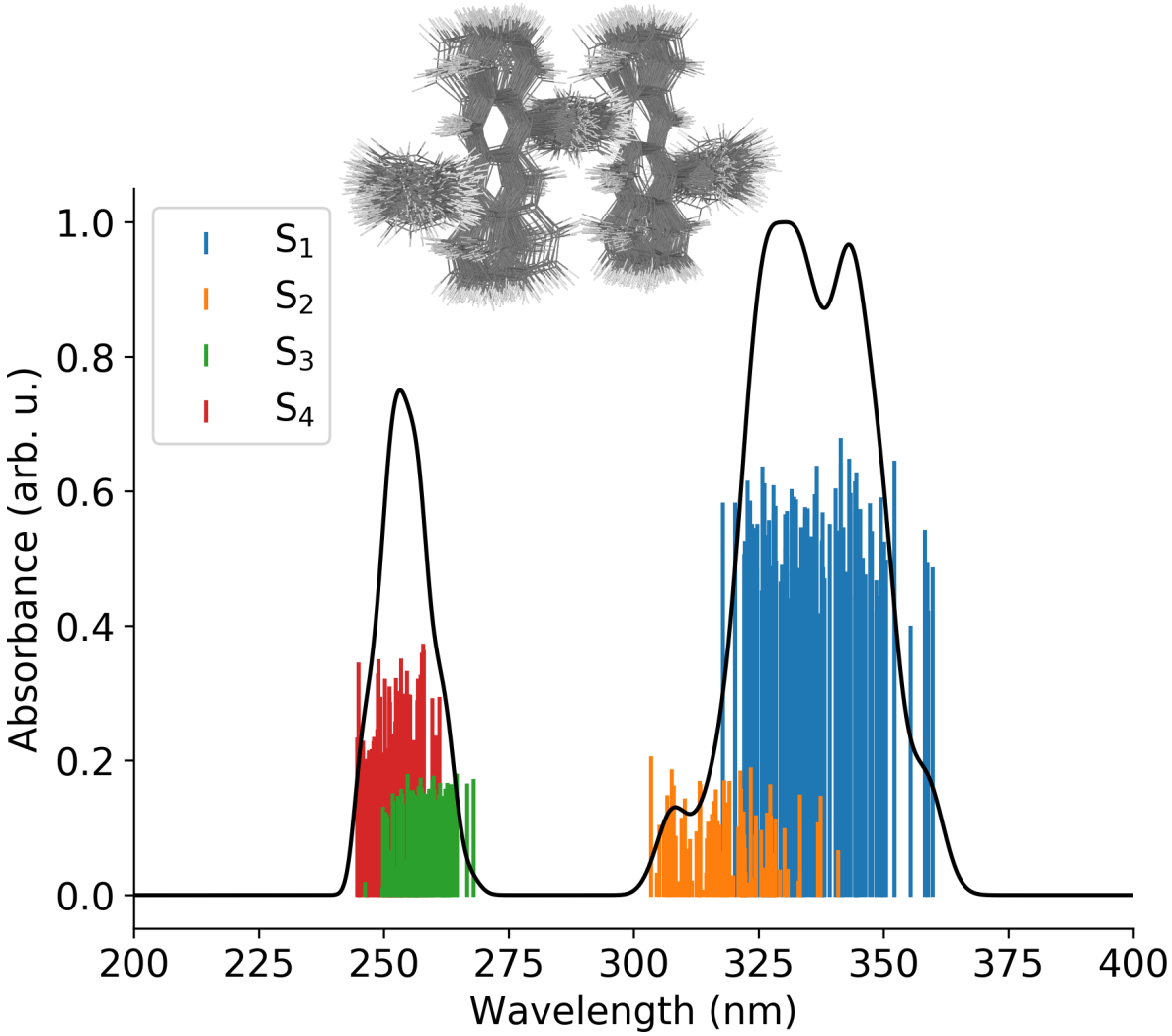

Figure S3: Absorption spectrum calculated using TD-lc-DFTB (30×30). Sticks are vertical absorption spectra for initial geometries (shown in the inset), and the black curve is the broadened spectrum calculated as $\sum_i f_i \exp\left(-\frac{1}{2\sigma^2}\left(\frac{1}{\lambda}-\frac{1}{\lambda_i}\right)^2\right)$ with $\sigma = 250\ \mathrm{cm}^{-1}$ and normalized to have maximum absorbance of 1 (here, λ is the wavelength, λ_i and f_i are computed excitation wavelengths and oscillator strengths, respectively, σ is a broadening parameter).

SI3 Additional analysis of dynamics

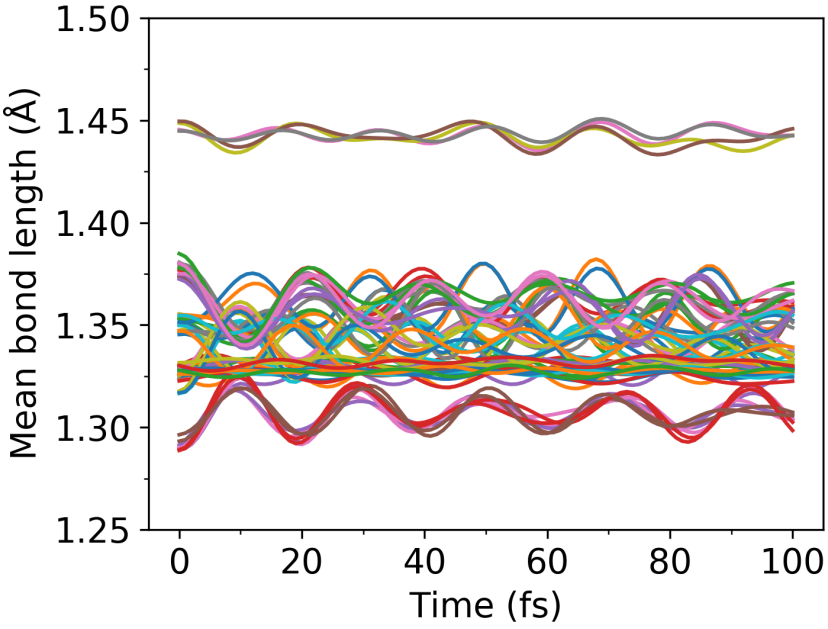

Figure S4: Time evolution of all CC bonds of the dimer, averaged over the whole ensemble of trajectories. Many CC bond lengths show oscillations with a period of ∼20 fs, what agrees very well with oscillations of $\mathrm{FTDM}_{\mathcal{H}(\mathcal{L})}$.

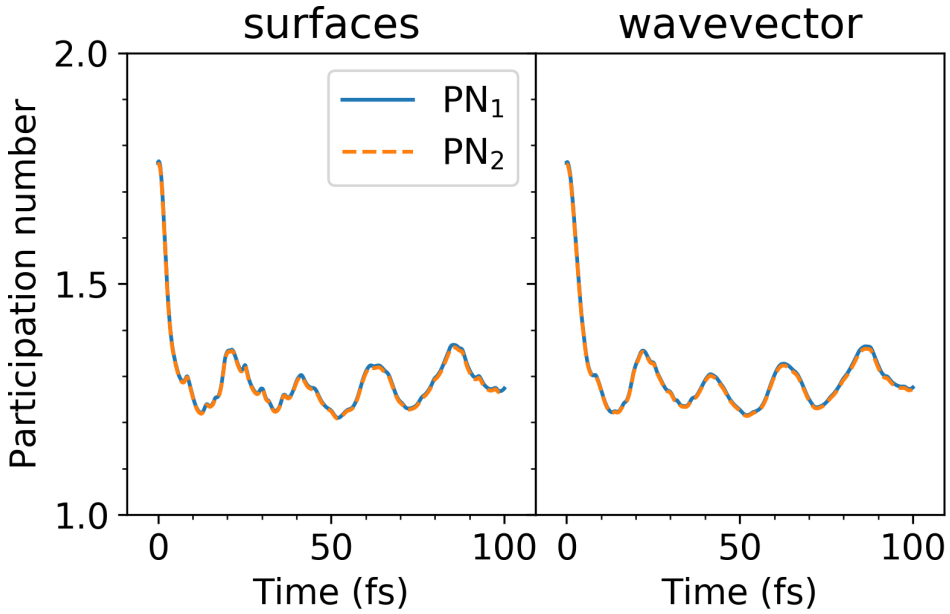

Figure S5: Participation numbers averaged over the swarm of trajectories. $\mathrm{PN}_1 = \left(\mathrm{FTDM}_{LL}^2 + \mathrm{FTDM}_{RR}^2\right)^{-1}$ and $\mathrm{PN}_2 = \left(\left(\mathrm{FTDM}_{LL} + \frac{\mathrm{FTDM}_{LR} + \mathrm{FTDM}_{RL}}{2}\right)^2 + \left(\frac{\mathrm{FTDM}_{RL} + \mathrm{FTDM}_{LR}}{2} + \mathrm{FTDM}_{RR}\right)^2\right)^{-1}$.

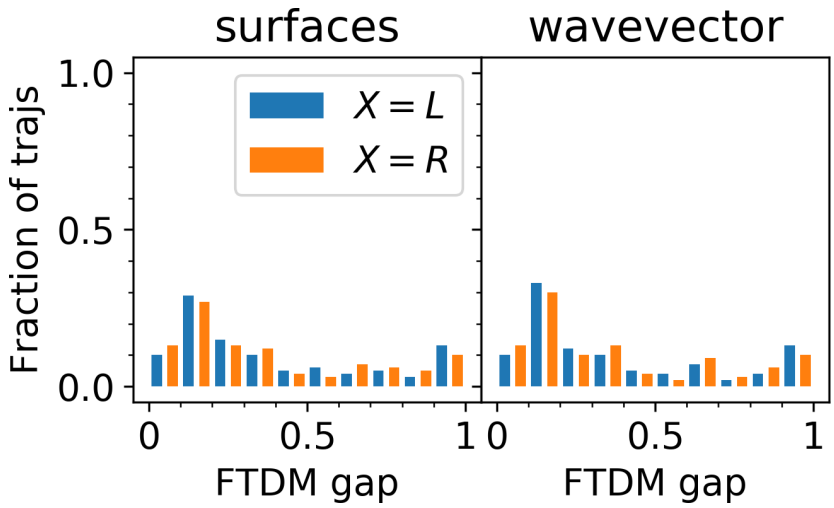

Figure S6: Distribution of trajectories over FTDM gap (calculated for 100 fs) for the L and R fragments.

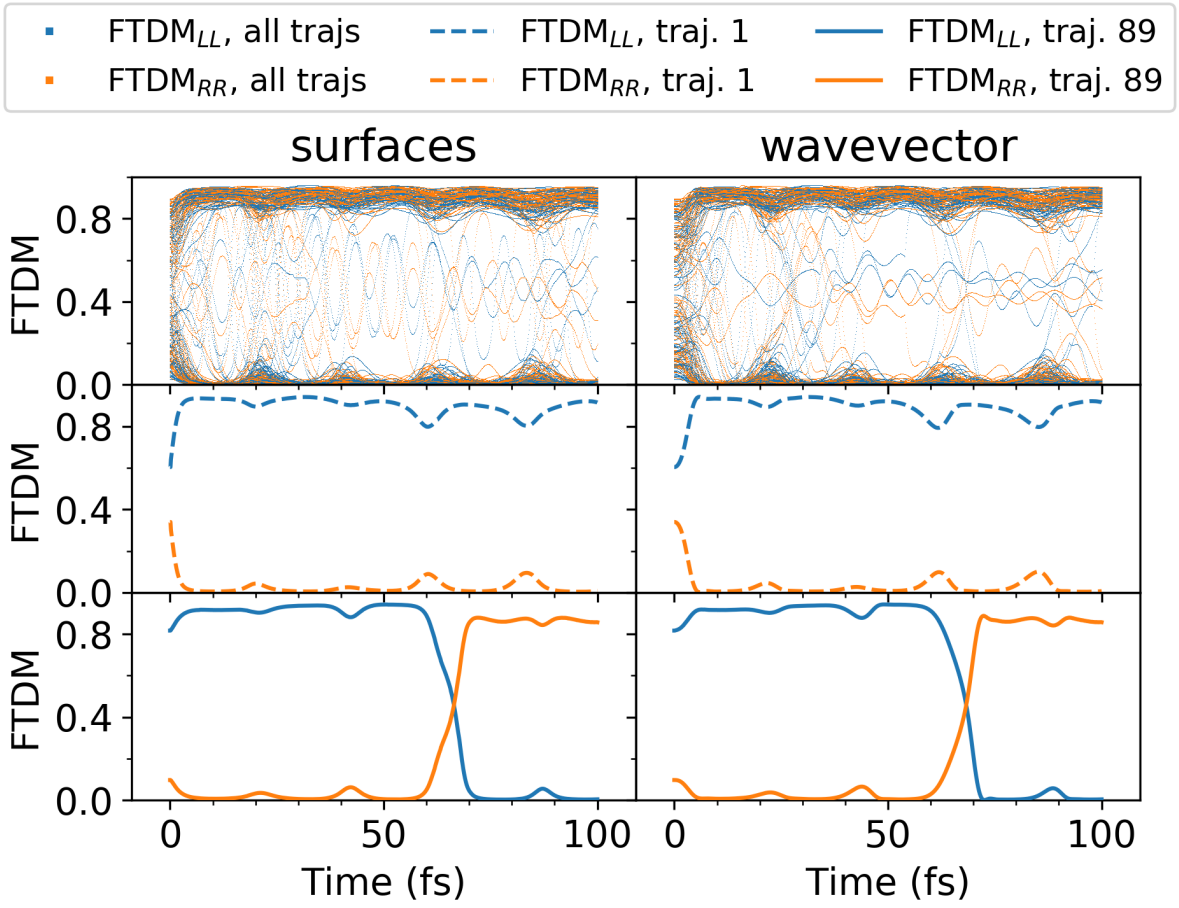

Figure S7: FTDM time evolutions for L and R fragments, for all trajectories (upper panels) and for two selected trajectories (middle and lower panels). The solid lines (lower panel) demonstrate the exciton transfer from L to R, whereas the dashed lines (middle panel) correspond to the exciton trapping (within 100 fs) on L.

SI4 Vibrationally-resolved $S_0 \rightarrow S_1$ spectrum of tetracene monomer

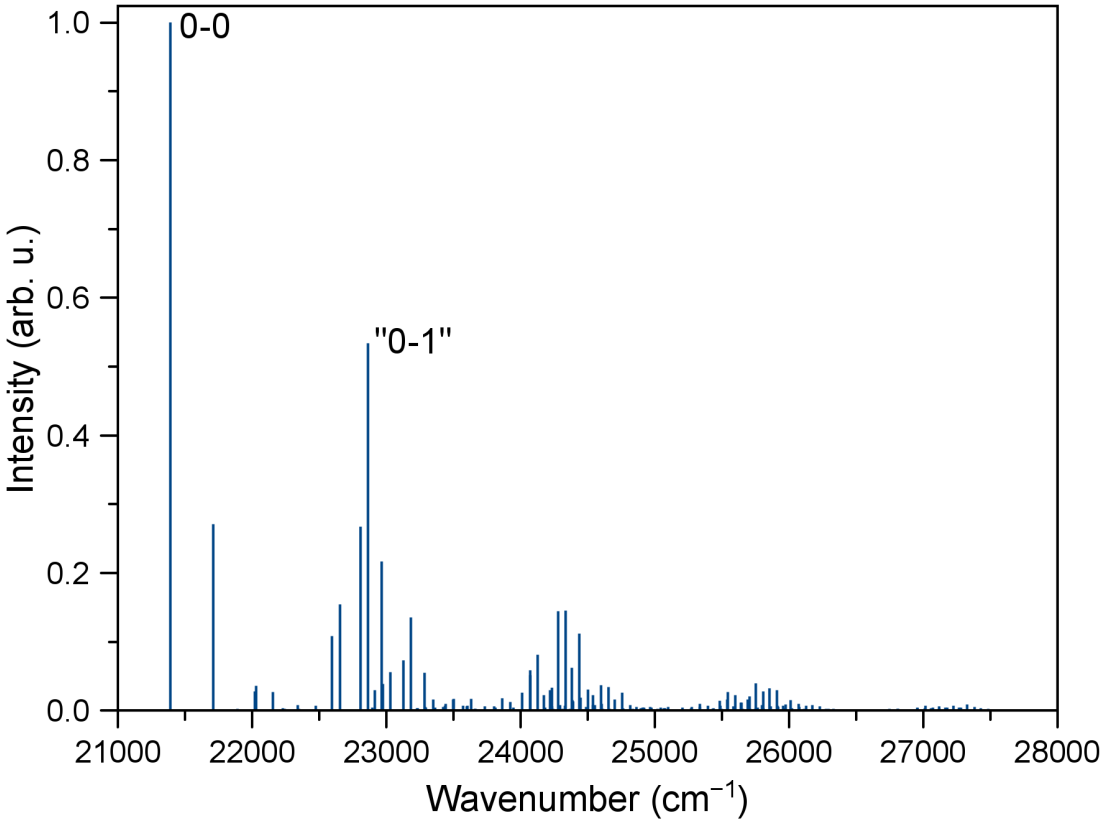

Figure S8: Vibrationally-resolved spectrum in the Franck–Condon approximation for the $S_0 \rightarrow S_1$ transition of the tetracene monomer computed on the (TD-)ωB97X-D/6-31G* level of theory.

SI5 Quantum description of the two-state model

The total molecular wave function in the diabatic representation is:

$$\Psi(\mathbf{r},\mathbf{Q},t) = \mathrm{X}_1^d(\mathbf{Q},t)\Phi_1^d(\mathbf{r}) + \mathrm{X}_2^d(\mathbf{Q},t)\Phi_2^d(\mathbf{r}) \tag{S1}$$

and in the adiabatic representation:

$$\Psi(\mathbf{r},\mathbf{Q},t) = \mathrm{X}_1^a(\mathbf{Q},t)\Phi_1^a(\mathbf{r};\mathbf{Q}) + \mathrm{X}_2^a(\mathbf{Q},t)\Phi_2^a(\mathbf{r};\mathbf{Q}) \tag{S2}$$

Here, $\mathbf{r}$ denotes electronic DoFs, $\mathbf{Q}$ vibrational DoFs, and t is time.

The adiabatic electronic states Φ^a are obtained from the diabatic ones Φ^d using the diabatic-to-adiabatic transformation (DAT) matrix as follows:[S22]

$$\begin{pmatrix}\Phi_1^a(\mathbf{r};\mathbf{Q})\\ \Phi_2^a(\mathbf{r};\mathbf{Q})\end{pmatrix} = \begin{pmatrix}-\sin(\alpha(\mathbf{Q})) & \cos(\alpha(\mathbf{Q}))\\ \cos(\alpha(\mathbf{Q})) & \sin(\alpha(\mathbf{Q}))\end{pmatrix}\begin{pmatrix}\Phi_1^d(\mathbf{r})\\ \Phi_2^d(\mathbf{r})\end{pmatrix} \tag{S3}$$

We note that this form of the DAT matrix (with $-\sin(\alpha(\mathbf{Q}))$ in the upper left corner) ensures that the $\Phi_1^a(\mathbf{r};\mathbf{Q})$ is the lower adiabatic state (S_1), whereas $\Phi_2^a(\mathbf{r};\mathbf{Q})$ is the upper adiabatic state (S_2), following the derivation of ref. S22. In (S3), the $\alpha(\mathbf{Q})$ is the so-called mixing or rotational angle, defined as:[S22]

$$\alpha(\mathbf{Q}) = \frac{1}{2}\arctan\left(\frac{2V_{12}(\mathbf{Q})}{V_{11}(\mathbf{Q}) - V_{22}(\mathbf{Q})}\right) \tag{S4}$$

SI6 Surface hopping results for the model system

In surface hopping, the time-dependent electronic wave function for trajectory i is expanded in the adiabatic basis:

$$\Phi_{el}^{i}(\mathbf{r},t;\mathbf{Q}_i(t)) = c_1^{a,i}(t)\Phi_1^a(\mathbf{r};\mathbf{Q}_i(t)) + c_2^{a,i}(t)\Phi_2^a(\mathbf{r};\mathbf{Q}_i(t)) \tag{S5}$$

Applying the DAT (S3), one can rewrite this expansion in the diabatic basis:

$$\begin{aligned}\Phi_{el}^{i}(\mathbf{r},t;\mathbf{Q}_i(t)) = &\left[-c_1^{a,i}(t)\sin\left(\alpha(\mathbf{Q}_i(t))\right) + c_2^{a,i}(t)\cos\left(\alpha(\mathbf{Q}_i(t))\right)\right]\Phi_1^d(\mathbf{r}) \\ &+ \left[c_1^{a,i}(t)\cos\left(\alpha(\mathbf{Q}_i(t))\right) + c_2^{a,i}(t)\sin\left(\alpha(\mathbf{Q}_i(t))\right)\right]\Phi_2^d(\mathbf{r})\end{aligned} \tag{S6}$$

In the "wavevector" method, the adiabatic populations are given by:

$$P_1^a(t) = \frac{1}{N}\sum_{i=1}^{N}\left|c_1^{a,i}(t)\right|^2 \tag{S7a}$$

$$P_2^a(t) = \frac{1}{N}\sum_{i=1}^{N}\left|c_2^{a,i}(t)\right|^2 \tag{S7b}$$

and the diabatic populations read:

$$P_1^d(t) = \frac{1}{N}\sum_{i=1}^{N}\left|-c_1^{a,i}(t)\sin\left(\alpha(\mathbf{Q}_i(t))\right) + c_2^{a,i}(t)\cos\left(\alpha(\mathbf{Q}_i(t))\right)\right|^2 \tag{S8a}$$

$$P_2^d(t) = \frac{1}{N}\sum_{i=1}^{N}\left|c_1^{a,i}(t)\cos\left(\alpha(\mathbf{Q}_i(t))\right) + c_2^{a,i}(t)\sin\left(\alpha(\mathbf{Q}_i(t))\right)\right|^2 \tag{S8b}$$

Here, N is the total number of trajectories.

In the "surfaces" method, the adiabatic populations are given by:

$$P_1^a(t) = \frac{N_1^a(t)}{N} \tag{S9a}$$

$$P_2^a(t) = \frac{N_2^a(t)}{N} \tag{S9b}$$

Here, $N_1^a(t)$ ($N_2^a(t)$) is the number of trajectories running on adiabatic surface 1 (2) at time t. The diabatic populations, in turn, are calculated as:

$$P_1^d(t) = \frac{1}{N}\sum_{i=1}^{N}\left[u_1^d(\lambda^i(t))\right]^2 \tag{S10a}$$

$$P_2^d(t) = \frac{1}{N}\sum_{i=1}^{N}\left[u_2^d(\lambda^i(t))\right]^2 \tag{S10b}$$

Here,

$$u_1^d(\lambda^i(t)) = \begin{cases}-\sin\left(\alpha(\mathbf{Q}_i(t))\right) & \text{if } \lambda^i(t)=1\\ \cos\left(\alpha(\mathbf{Q}_i(t))\right) & \text{if } \lambda^i(t)=2\end{cases} \tag{S11a}$$

$$u_2^d(\lambda^i(t)) = \begin{cases}\cos\left(\alpha(\mathbf{Q}_i(t))\right) & \text{if } \lambda^i(t)=1\\ \sin\left(\alpha(\mathbf{Q}_i(t))\right) & \text{if } \lambda^i(t)=2\end{cases} \tag{S11b}$$

and $\lambda^i(t)$ is the current adiabatic surface of trajectory i.

Further, for each trajectory i at time t we define the *highest* ($\mathcal{H}$) fragment with the diabatic probability $p_{\mathcal{H}}^{d,i}$ as

$$p_{\mathcal{H}}^{d,i}(t) = \max\left(\left[u_1^d(\lambda^i(t))\right]^2, \left[u_2^d(\lambda^i(t))\right]^2\right) \tag{S12}$$

in the case of the "surfaces" method and

$$\begin{aligned} p_{\mathcal{H}}^{d,i}(t) = \max\Big(&\left|-c_1^{a,i}(t)\sin\left(\alpha(\mathbf{Q}_i(t))\right) + c_2^{a,i}(t)\cos\left(\alpha(\mathbf{Q}_i(t))\right)\right|^2, \\ &\left|c_1^{a,i}(t)\cos\left(\alpha(\mathbf{Q}_i(t))\right) + c_2^{a,i}(t)\sin\left(\alpha(\mathbf{Q}_i(t))\right)\right|^2\Big) \end{aligned} \tag{S13}$$

in the case of the "wavevector" method. Finally, we average the diabatic probabilities of the highest fragment over the swarm of trajectories to obtain the diabatic population of the highest fragment:

$$P_{\mathcal{H}}^d(t) = \frac{1}{N}\sum_{i=1}^{N} p_{\mathcal{H}}^{d,i}(t) \tag{S14}$$

Besides "surfaces" and "wavevector" methods, the diabatic populations can (and should) be computed using a method that uses a nuclear-electronic density matrix, as proposed by the group of Subotnik.[S23] We will term this method "mixed" (see Method 3 in ref. S23). Using eq. (11) of ref. S23, we obtain:

$$\begin{aligned} P_1^d(t) = \frac{1}{N}\sum_{i=1}^{N}\Big(&\left[-\sin\left(\alpha(\mathbf{Q}_i(t))\right)\right]^2\delta_{1,\lambda^i(t)} + \left[\cos\left(\alpha(\mathbf{Q}_i(t))\right)\right]^2\delta_{2,\lambda^i(t)} \\ &-\sin\left(\alpha(\mathbf{Q}_i(t))\right)\cos\left(\alpha(\mathbf{Q}_i(t))\right)2\Re\left(c_1^{a,i}(t)c_2^{a,i*}(t)\right)\Big) \end{aligned} \tag{S15a}$$

$$\begin{aligned} P_2^d(t) = \frac{1}{N}\sum_{i=1}^{N}\Big(&\left[\cos\left(\alpha(\mathbf{Q}_i(t))\right)\right]^2\delta_{1,\lambda^i(t)} + \left[\sin\left(\alpha(\mathbf{Q}_i(t))\right)\right]^2\delta_{2,\lambda^i(t)} \\ &+\cos\left(\alpha(\mathbf{Q}_i(t))\right)\sin\left(\alpha(\mathbf{Q}_i(t))\right)2\Re\left(c_1^{a,i}(t)c_2^{a,i*}(t)\right)\Big) \end{aligned} \tag{S15b}$$

Here, δ is the Kronecker delta.

Again, one can define the $\mathcal{H}$ fragment by:

$$\begin{aligned} p_{\mathcal{H}}^{d,i}(t) = \max\Big\{&\Big(\left[-\sin\left(\alpha(\mathbf{Q}_i(t))\right)\right]^2\delta_{1,\lambda^i(t)} + \left[\cos\left(\alpha(\mathbf{Q}_i(t))\right)\right]^2\delta_{2,\lambda^i(t)} \\ &-\sin\left(\alpha(\mathbf{Q}_i(t))\right)\cos\left(\alpha(\mathbf{Q}_i(t))\right)2\Re\left(c_1^{a,i}(t)c_2^{a,i*}(t)\right)\Big), \\ &\Big(\left[\cos\left(\alpha(\mathbf{Q}_i(t))\right)\right]^2\delta_{1,\lambda^i(t)} + \left[\sin\left(\alpha(\mathbf{Q}_i(t))\right)\right]^2\delta_{2,\lambda^i(t)} \\ &+\cos\left(\alpha(\mathbf{Q}_i(t))\right)\sin\left(\alpha(\mathbf{Q}_i(t))\right)2\Re\left(c_1^{a,i}(t)c_2^{a,i*}(t)\right)\Big)\Big\} \end{aligned} \tag{S16}$$

and average over the swarm of trajectories using eq. (S14).

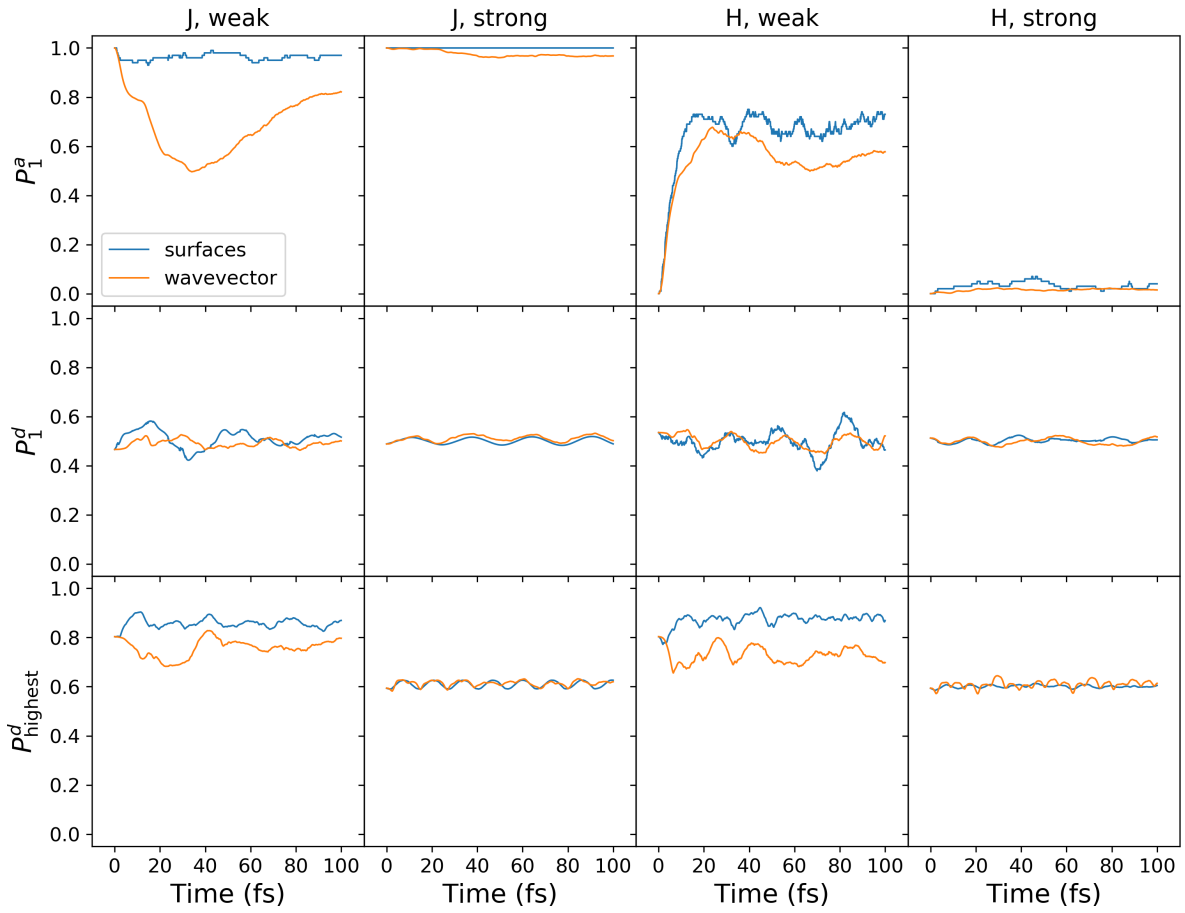

Figure S9: Surface hopping calculations *without decoherence correction* for the model system. Shown are the results for the J- and H-aggregates with weak and strong diabatic coupling.

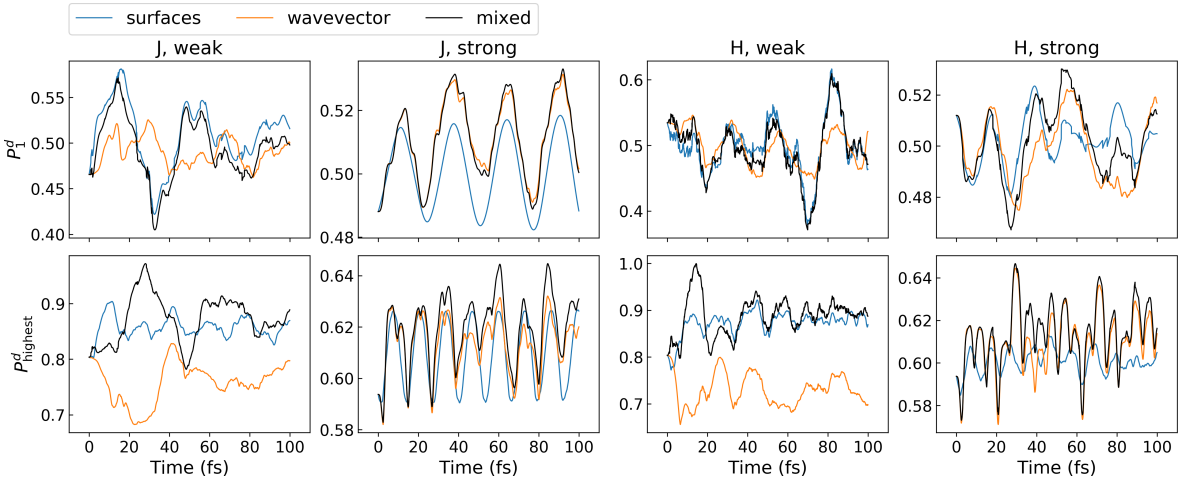

Figure S10: Comparison of "surfaces", "wavevector", and "mixed" diabatic populations. The surface hopping calculations were done *without decoherence correction*.

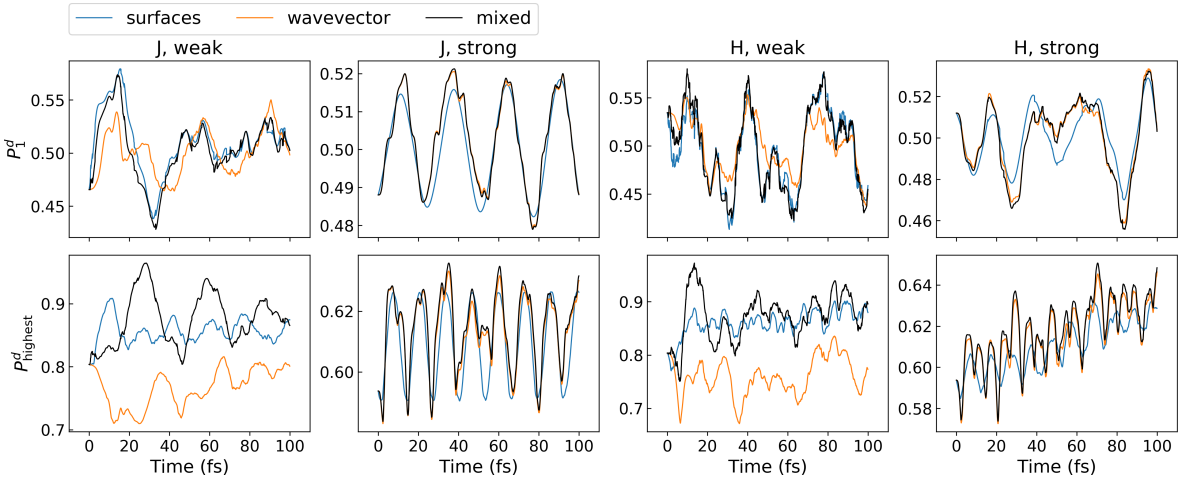

Figure S11: Comparison of "surfaces", "wavevector", and "mixed" diabatic populations. The surface hopping calculations were done *with decoherence correction*.

SI7 Lowest vibronic state

To have a measure of a relaxed state, we obtained the lowest vibronic (lv) state of the weakly coupled J-aggregate by numerical diagonalization of Hamiltonian (eq. (4) of the main text) using the discrete variable representation (DVR) of Colbert and Miller.[S24] The used grid for the DVR comprised 10000 points (100 points between -0.3 and 0.5 in the Q_1 direction and the same in the Q_2 direction). The lv state is $\Psi^{lv}(\mathbf{r},\mathbf{Q}) = \mathrm{X}_1^{d,(lv)}(\mathbf{Q})\Phi_1^d(\mathbf{r}) + \mathrm{X}_2^{d,(lv)}(\mathbf{Q})\Phi_2^d(\mathbf{r})$. The diabatic nuclear wave functions $\mathrm{X}_1^{d,(lv)}(\mathbf{Q})$ and $\mathrm{X}_2^{d,(lv)}(\mathbf{Q})$ as well the nuclear probability density $\int \left|\Psi^{lv}(\mathbf{r},\mathbf{Q})\right|^2 \mathrm{d}\mathbf{r} = \left|\mathrm{X}_1^{d,(lv)}(\mathbf{Q})\right|^2 + \left|\mathrm{X}_2^{d,(lv)}(\mathbf{Q})\right|^2$ are shown in Fig. S12.

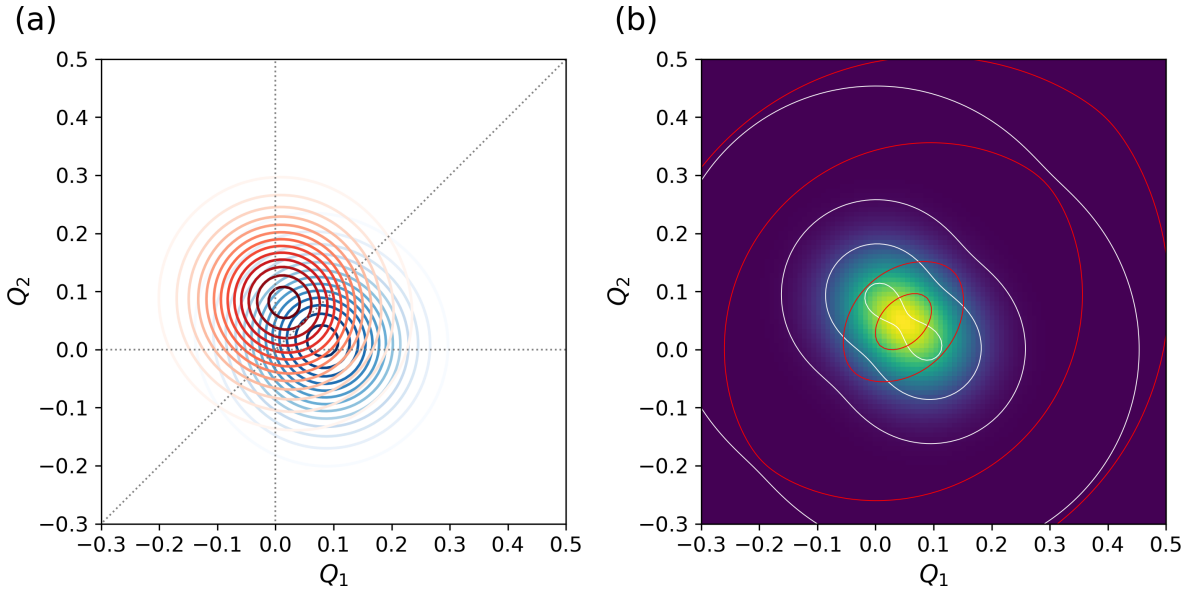

Figure S12: (a) Diabatic nuclear wave functions of the lowest vibronic (lv) state of the weakly coupled J-aggregate. $\mathrm{X}_1^{d,(lv)}(\mathbf{Q})$ is shown in blue, $\mathrm{X}_2^{d,(lv)}(\mathbf{Q})$ is shown in red. (b) The heat map shows nuclear probability density $\left|\mathrm{X}_1^{d,(lv)}(\mathbf{Q})\right|^2 + \left|\mathrm{X}_2^{d,(lv)}(\mathbf{Q})\right|^2$ of the lowest vibronic state; the white contours show the lower adiabatic potential energy surface (PES), and the red contours show the upper adiabatic PES.

SI8 Dynamics starting from a localized state

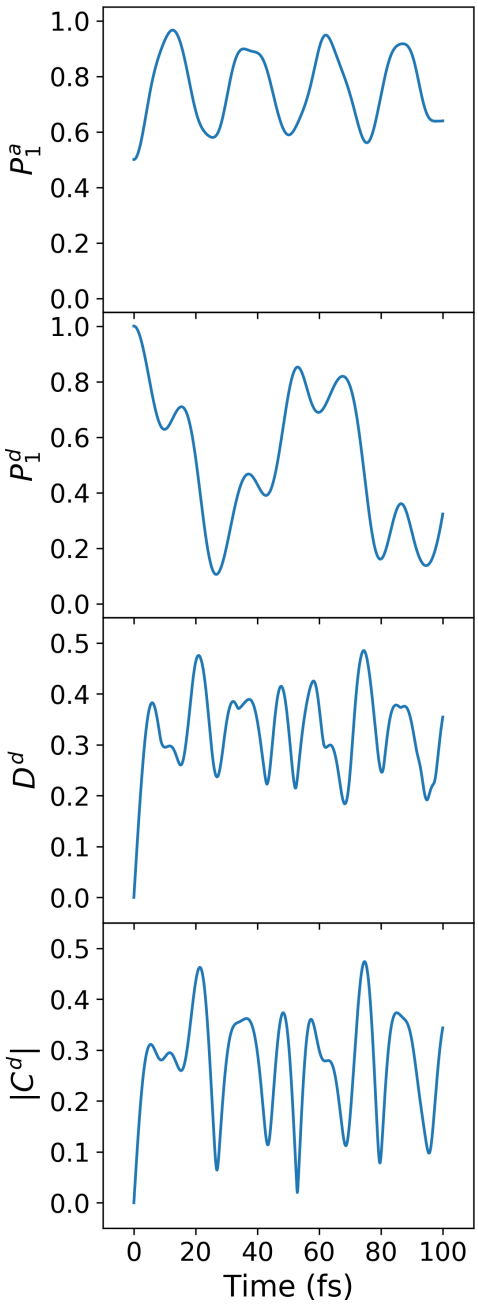

Figure S13: Quantum dynamics results for the weakly coupled J-aggregate and the localized initial excitation to the Φ_1^d state.

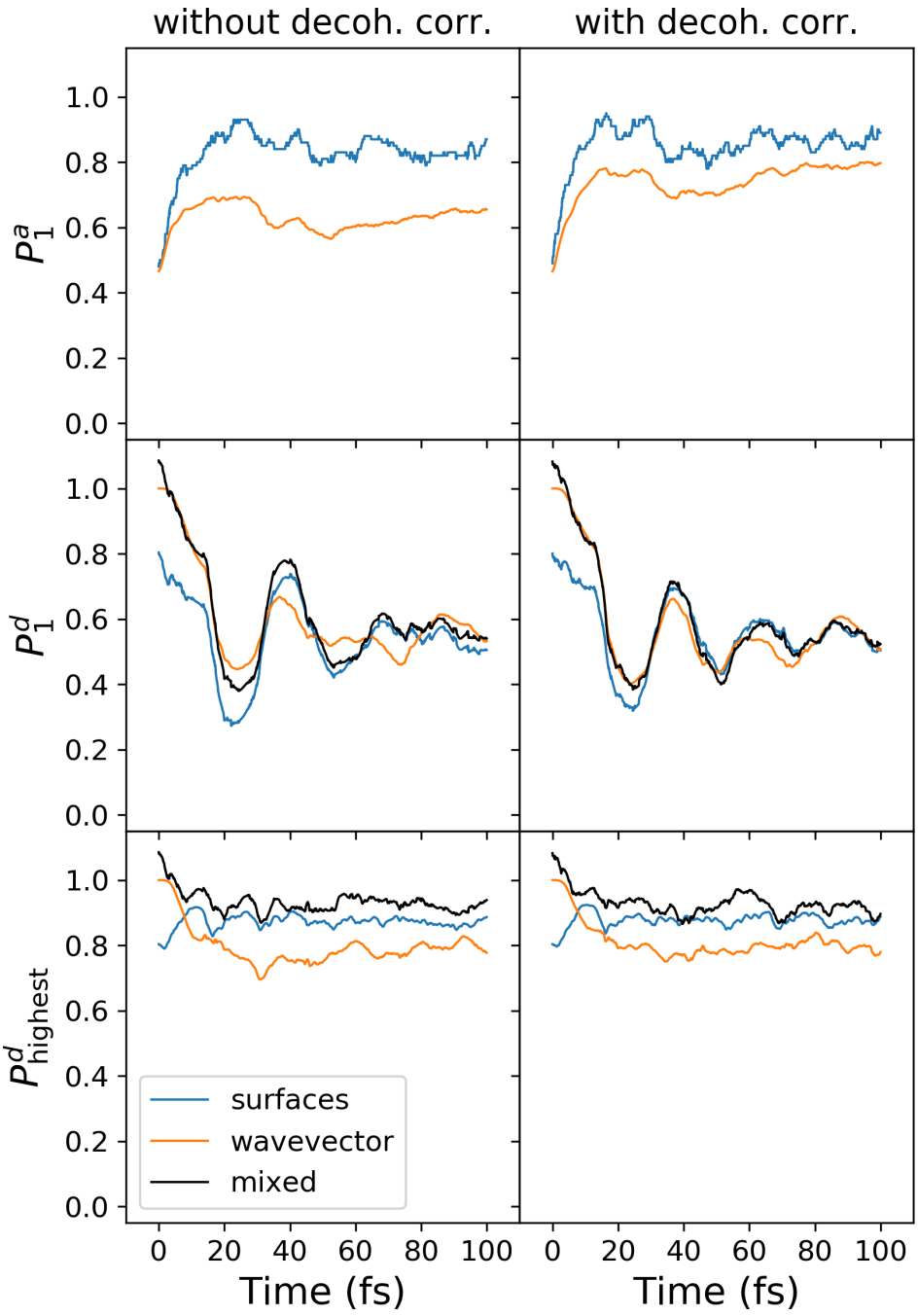

Figure S14: Surface hopping results for the weakly coupled J-aggregate and the localized initial excitation to the Φ_1^d state. The initial coefficients $c_{1(2)}^{a,i}(t=0)$ were determined employing the DAT, $\Phi_1^d = -\sin\left(\alpha(\mathbf{Q}_i(t=0))\right)\Phi_1^a + \cos\left(\alpha(\mathbf{Q}_i(t=0))\right)\Phi_2^a$, *i.e.* $c_1^{a,i}(t=0) = -\sin\left(\alpha(\mathbf{Q}_i(t=0))\right)$ and $c_2^{a,i}(t=0) = \cos\left(\alpha(\mathbf{Q}_i(t=0))\right)$. The initial adiabatic surface was chosen by comparing the calculated coefficients, *i.e.* a trajectory is launched on adiabat 1 if $|c_1^{a,i}(t=0)| > |c_2^{a,i}(t=0)|$, and on adiabat 2 otherwise. Note that only the "wavevector" method yields correct diabatic populations at $t = 0$.

References

[S1] M. E. Casida, in *Time-Dependent Density Functional Response Theory for Molecules*, World Scientific, 1995, pp. 155–192.

[S2] A. D. Becke, *J. Chem. Phys.*, 1993, **98**, 5648–5652.

[S3] P. J. Stephens, F. J. Devlin, C. F. Chabalowski and M. J. Frisch, *J. Phys. Chem.*, 1994, **98**, 11623–11627.

[S4] T. Yanai, D. P. Tew and N. C. Handy, *Chem. Phys. Lett.*, 2004, **393**, 51–57.

[S5] J.-D. Chai and M. Head-Gordon, *Phys. Chem. Chem. Phys.*, 2008, **10**, 6615–6620.

[S6] A. D. McLachlan and M. A. Ball, *Rev. Mod. Phys.*, 1964, **36**, 844–855.

[S7] J. Schirmer, *Phys. Rev. A*, 1982, **26**, 2395–2416.

[S8] O. Christiansen, H. Koch and P. Jørgensen, *Chem. Phys. Lett.*, 1995, **243**, 409–418.

[S9] M. J. Frisch, G. W. Trucks, H. B. Schlegel, G. E. Scuseria, M. A. Robb, J. R. Cheeseman, G. Scalmani, V. Barone, G. A. Petersson, H. Nakatsuji, X. Li, M. Caricato, A. V. Marenich, J. Bloino, B. G. Janesko, R. Gomperts, B. Mennucci, H. P. Hratchian, J. V. Ortiz, A. F. Izmaylov, J. L. Sonnenberg, D. Williams-Young, F. Ding, F. Lipparini, F. Egidi, J. Goings, B. Peng, A. Petrone, T. Henderson, D. Ranasinghe, V. G. Zakrzewski, J. Gao, N. Rega, G. Zheng, W. Liang, M. Hada, M. Ehara, K. Toyota, R. Fukuda, J. Hasegawa, M. Ishida, T. Nakajima, Y. Honda, O. Kitao, H. Nakai, T. Vreven, K. Throssell, J. A. Montgomery, Jr., J. E. Peralta, F. Ogliaro, M. J. Bearpark, J. J. Heyd, E. N. Brothers, K. N. Kudin, V. N. Staroverov, T. A. Keith, R. Kobayashi, J. Normand, K. Raghavachari, A. P. Rendell, J. C. Burant, S. S. Iyengar, J. Tomasi, M. Cossi, J. M. Millam, M. Klene, C. Adamo, R. Cammi, J. W. Ochterski, R. L. Martin, K. Morokuma, O. Farkas, J. B. Foresman and D. J. Fox, *Gaussian 16 Revision A.03*, 2016, Gaussian Inc. Wallingford CT.

[S10] *TURBOMOLE V7.0 2015, a development of University of Karlsruhe and Forschungszentrum Karlsruhe GmbH, 1989-2007, TURBOMOLE GmbH, since 2007; available from* `http://www.turbomole.com`.

[S11] F. Weigend and R. Ahlrichs, *Phys. Chem. Chem. Phys.*, 2005, **7**, 3297–3305.

[S12] T. H. Dunning, *J. Chem. Phys.*, 1989, **90**, 1007–1023.

[S13] H. Liu, R. Wang, L. Shen, Y. Xu, M. Xiao, C. Zhang and X. Li, *Org. Lett.*, 2017, **19**, 580–583.

[S14] E. Titov, A. Humeniuk and R. Mitrić, *Phys. Chem. Chem. Phys.*, 2018, **20**, 25995–26007.

[S15] D. J. Tozer, R. D. Amos, N. C. Handy, B. O. Roos and L. Serrano-Andrés, *Mol. Phys.*, 1999, **97**, 859–868.

[S16] L. Bernasconi, M. Sprik and J. Hutter, *J. Chem. Phys.*, 2003, **119**, 12417–12431.

[S17] A. Dreuw, J. L. Weisman and M. Head-Gordon, *J. Chem. Phys.*, 2003, **119**, 2943–2946.

[S18] A. Dreuw and M. Head-Gordon, *J. Am. Chem. Soc.*, 2004, **126**, 4007–4016.

[S19] R. J. Magyar and S. Tretiak, *J. Chem. Theory Comput.*, 2007, **3**, 976–987.

[S20] E. Sagvolden, F. Furche and A. Köhn, *J. Chem. Theory Comput.*, 2009, **5**, 873–880.

[S21] E. Titov and P. Saalfrank, *J. Phys. Chem. A*, 2016, **120**, 3055–3070.

[S22] G. J. Atchity, S. S. Xantheas and K. Ruedenberg, *J. Chem. Phys.*, 1991, **95**, 1862–1876.

[S23] B. R. Landry, M. J. Falk and J. E. Subotnik, *J. Chem. Phys.*, 2013, **139**, 211101.

[S24] D. T. Colbert and W. H. Miller, *J. Chem. Phys.*, 1992, **96**, 1982–1991.